



# Structural response of a cable-stayed bridge subjected to lateral seismic excitations

Amr Z. Elkady<sup>1,2</sup> · Maryam A. Seleemah<sup>3</sup> · Farhad Ansari<sup>4</sup>

Received: 20 February 2018 / Accepted: 13 April 2018 / Published online: 20 April 2018  
© Springer-Verlag GmbH Germany, part of Springer Nature 2018

## Abstract

Cable-stayed bridges are structurally efficient and offer cost effective solutions in medium to large-span crossings. The study reported in this article aimed at determining the behavior of a typical cable-stayed bridge when subjected to lateral earthquake excitations. A hybrid analytical–experimental technique is introduced to experimentally simulate the earthquake excitations on the bridge. In this technique, displacement time history of the bridge mid-span was first obtained analytically by exciting the bridge using the earthquake acceleration records. To experimentally simulate the earthquake excitations, these displacements were applied on a  $\frac{1}{60}$  scale model of a single plane cable-stayed bridge using a displacement controlled shaker. The efficiency of this technique was evaluated by comparing the experimental versus analytical response in terms of dynamic characteristics and displacement responses of the bridge. The analytical response of the bridge served as a verification tool for validation of key response parameters of the full-scale bridge. These parameters included forces in cables, strains and stresses in the deck, and moments and shear forces acting on pylons in the transverse direction.

**Keywords** Cable-stayed bridges · Earthquakes · Lateral excitations · Resonance · Fiber Bragg grating (FBG) · Structural health monitoring

## 1 Introduction

Bridges are considered one of the core elements of the public works infrastructure system and they are intrinsic to most sectors of industrial productivity. While performance

of the bridges is directly linked to the economic development, the consequences of their failures are serious and associated with loss of life and injuries [7, 9]. For instance, the failure of the Ohio Silver Bridge in 1967 was responsible for 46 deaths, and in 2007 the collapse of the I-35 W Bridge in Minnesota caused 13 deaths and injured another 145 [14]. Lessons learnt from such unfortunate bridge failures go back several decades and they have been responsible for some major changes to the design codes. Passive approach in understanding the behavior of larger bridges although useful has been incremental and not sufficient for thorough understanding of the bridge response to sophisticated loading patterns. The complexity of modern structural systems and the use of newer materials as well as the recent surge in frequency of natural disasters, such as earthquakes, storm surges, and hurricanes, call for holistic approaches for understanding the structural response of the large bridges.

Cable-stayed bridges are structurally efficient, esthetically pleasing, and offer cost effective alternatives for carrying the loads in medium to large-span crossings. They

---

✉ Farhad Ansari  
fansari@uic.edu

Amr Z. Elkady  
aelkad2@uic.edu

Maryam A. Seleemah  
maryam.seleemah@gmail.com

<sup>1</sup> Faculty of Engineering, Tanta University, Tanta, Egypt

<sup>2</sup> Visiting Researcher at the Department of Civil and Materials Engineering, University of Illinois, Chicago, IL 60607, USA

<sup>3</sup> Department of Structural Engineering, Faculty of Engineering, Tanta University, Tanta, Egypt

<sup>4</sup> Christopher B. and Susan S. Burke Distinguished Professor, Department of Civil and Materials Engineering, University of Illinois at Chicago, Chicago, IL 60607, USA

offer effective alternatives to suspension bridges in locations where insufficient space does not allow for use of anchorages at the abutments. In general, all large-span bridges are vulnerable to lateral dynamic loads, such as forces due to wind pressures and earthquake motions. In the case of cable-stayed and suspension bridges, interaction between the primary load carrying members such as the decks and pylons and force transmission elements such as cables adds to the complexities of the dynamic response of such bridges [15]. Especially, due to reduced modal frequencies, cable-stayed bridges are more sensitive to earthquakes and wind forces. In general, earthquake loads and wind pressures are the primary control loads in design of large-span bridges. Ambient vibration tests (AVT) have been one of the prevalent techniques employed for assessing the dynamic properties of bridges. During the tests, acceleration of bridge elements at pre-selected locations is measured when the bridge is only subjected to ambient loads. At the analysis stage, the computation of bridge dynamic properties relies on alternative output-only modal identification techniques, either parametric or non-parametric, all of which assume a white noise excitation input [6, 8].

Significant research efforts have been made to model the behavior of the bridges under different dynamic load excitations [17]. For example, Caetano and Cunha investigated dynamic cable–deck interaction in a physical model of a cable-stayed bridge [1]. They showed that energy can be transferred by vibration of the cables between the deck and the towers during earthquakes. Siringoringo and Fujino studied the dynamic performance of the Yokohama-Bay Bridge utilizing system identification techniques for understanding the global response of the bridge by estimating modal parameters [16]. Liu et al. investigated the use of viscous dampers to dissipate the kinetic energy of Hangzhou Bay cable-stayed bridge both transversely and longitudinally [11]. Camara and Astiz studied the applicability of nonlinear dynamic (NL-RHA) and static (pushover) procedures in the study of the nonlinear seismic behavior of cable-stayed bridges [2].

Review of technical literature reveals that only a limited number of studies focused their goal on studying the lateral seismic response of cable-stayed bridges. In essence, the effects of direct interaction between the bridge members subjected to seismic motions are potentially significant, especially in the lateral direction. For example, Chang et al. studied the causes of damage in Chi-Lu cable-stayed bridge [4]. The damage in the bridge tower during the Chi-Chi earthquake (Taiwan 1999) was attributed to the lateral excitations of the bridge and one of the most severe cases of seismic damage reported in a cable-stayed bridge. Camara et al. demonstrated that, in such bridges, the deck and the tower have to be rigidly connected in the lateral

direction to control the displacements of the tower under wind and seismic actions [3]. The deck–tower reaction was observed to increase the transverse bending moments and shear forces in the towers, making the lateral components of the seismic motions more demanding than the longitudinal and vertical directions. Furthermore, their study indicated the key roles of different vibration modes on the dynamic interaction between the deck and the towers of cable-stayed bridges. An extensive parametric analysis was proposed to address the influence of the main span length, the tower geometry, the cable-system arrangement, the width and height of the deck and the soil conditions. It was demonstrated that the vibration modes that govern the seismic response of cable-stayed bridges in the transverse direction involve the interaction between the tower and the deck, but the order of these modes and the parts of the deck that are affected change with the main span length. It was also observed that the interaction between the deck and the towers during the earthquake is maximized if their isolated vibration frequencies are close to each other, leading to a significantly larger seismic demand.

Recent studies have been focused on structural health monitoring and safety evaluation of cable-stayed bridges. In assessing the structural health during field tests of a bridge, the modal properties of the structure are measured at limited numbers of accessible locations [10, 19]. To optimize the measurement efforts, the number of degrees of freedom (DOFs) of the mass and stiffness matrices obtained from the numerical analysis is reduced to a reasonable number of sensors at desired directions.

This article pertains to a study that aimed at determining the behavior of a typical cable-stayed bridge when subjected to lateral earthquake excitations. The realistic approach involved fabrication and testing of a scaled model of an actual bridge to facilitate application of the transverse seismic excitations. A hybrid analytical–experimental technique was employed to simulate the earthquake excitations. In this technique, displacement time history of the mid-span of the bridge was first obtained analytically by exciting the bridge using the earthquake acceleration records. Then, the excitations were experimentally simulated on the scaled model of the bridge using a displacement controlled shaker at the mid-span of the bridge. The efficiency of this technique was evaluated by monitoring the bridge response in terms of bridge strains, displacements, and accelerations. The experimental response of the bridge served as a resource for verification of analytical model of the full-scale bridge. Key response parameters included forces in cables, strains and stresses in the deck, as well as moments and shear forces acting on the pylons in the transverse direction.



**Fig. 1** Chongqing Dongshuimen Yangtze River Bridge, China, (<http://www.crbbg.com>)

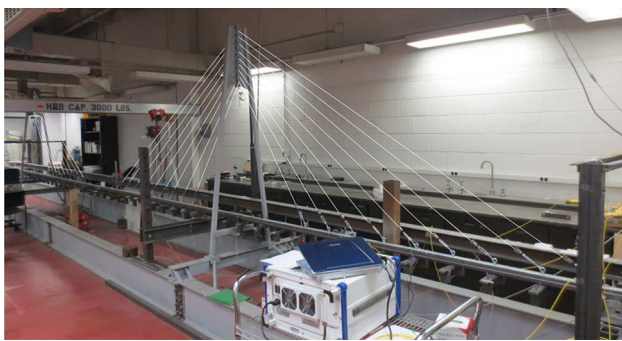


**Fig. 2** Model bridge in the lab

## 2 Equations of motion

The fundamental equations employed for the computation of the response of the cable-stayed bridge to dynamic motions are provided herein. The cable-stayed bridge is considered a multi-degree of freedom system. It is assumed to remain elastic with unconstrained degrees of freedom, except for the constraints at support locations [18]. The displacement of the base of the structure in time domains is given by

$$u^t(t) = u_g(t) + u(t), \tag{1}$$

where  $u_g$  is the displacement of the ground,  $u^t$  is the total displacement of the mass of the structure, and  $u$  is the relative displacement between the mass and the ground.

The dynamic equation of equilibrium, considering only free vibration is

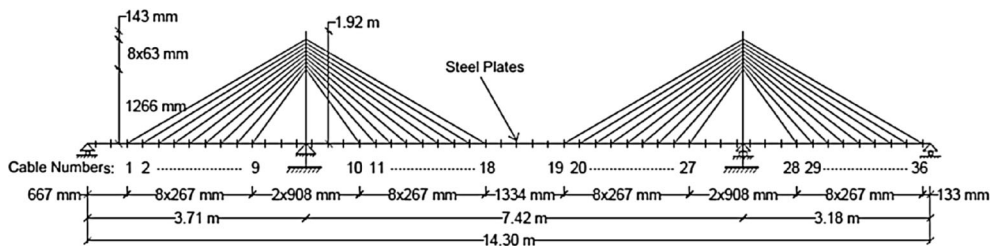
$$f_i + f_D + f_s = 0, \tag{2}$$

where  $f_i$  is the inertia force =  $[M]\{\ddot{U}\}$ ,  $f_D$  is the damping force =  $[C_u]\{\dot{U}\}$  and  $f_s$  is the stiffness force =  $[K]\{U\}$ .

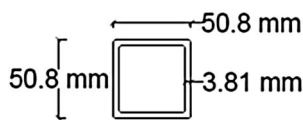
The equation of motion due to seismic ground excitations can be written in the following form:

$$[M]\{\ddot{U}\} + [C_u]\{\dot{U}\} + [K]\{U\} = -[M]\{R\}\ddot{u}_g, \tag{3}$$

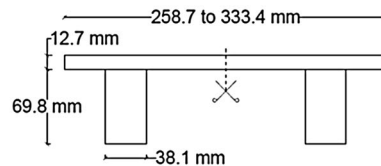
where  $[M]$ ,  $[C_u]$ , and  $[K]$  are the lumped mass, damping and stiffness matrices, respectively.  $\{U\}$ ,  $\{\dot{U}\}$ , and  $\{\ddot{U}\}$  are the vectors of relative displacements, velocities and accelerations, respectively, and  $\{R\}$  is the unit vector.



**(a)** Schematic and dimension of the model



**(b)** Cross-section of deck



**(c)** Steel plates to consider the dead load

**Fig. 3** Structural model of cable-stayed bridge

**Table 1** Similitude requirements for elastic vibrations

Parameter	Dimensions (engineering units)	Scaling factors	
		Exact	Current study
Linear dimension	L	60	60
Displacement	L	60	60
Time	T	7.746	1
Force	F	3600	3600
Bending moment	FL	216,000	216,000
Gravitational acceleration	LT <sup>-2</sup>	1	1
Modulus of elasticity	FL <sup>-2</sup>	1	1
Stress	FL <sup>-2</sup>	1	1
Poisson ratio	–	1	1

### 3 Experimental program

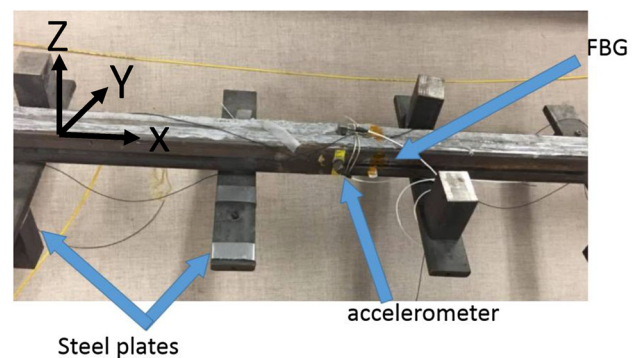
The experimental program involved testing of a scaled model of an actual cable-stayed bridge. The  $\frac{1}{60}$  laboratory scale model of Chongqing Dongshuimen Yangtze River Bridge was employed for the laboratory experiments (Fig. 1). The main bridge is a double-tower single-cable plane cable-stayed steel truss Girder Bridge, with three spans of 222.5, 445, and 190.5 m, respectively. This bridge was selected because the owners of the bridge had provided access to the bridge plans during the construction of the bridge in cooperation with an international research program [12, 13]. Figure 2 shows the photo of the bridge in the laboratory. Schematic diagram and dimensions of the model and the cross-section of deck are shown in Fig. 3.

The  $\frac{1}{60}$  scaling factor was employed based on the elastic direct method for scaling the structure. In direct modeling, strains and deformations are representative of similar quantities of the prototype structure under the same loading conditions and they are built as a geometric similitude of the prototype cross-section [20]. A hollow boxed cross-section was utilized for the structural model to simulate the shape of the prototype cross-section (Fig. 3b). The yield strength of the steel employed for the construction of the deck and the pylons was 235 MPa. Steel piano wires with tensile strength of 2500 MPa and a diameter of 0.4 mm were employed for the bridge cables. Fixed bases were used in the pylons supports. The two pylons have a moment of inertia of 132,248 mm<sup>4</sup>. To adequately represent the dead load of the bridge, additional steel elements were attached to the deck at equal intervals (Fig. 3c).

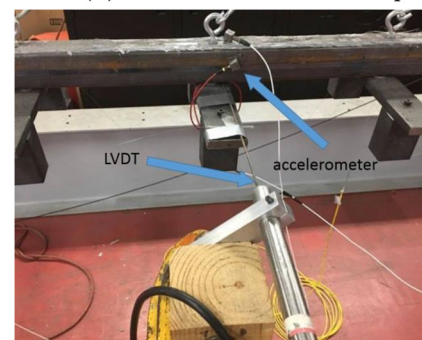
The similitude requirements of elastic structures under earthquake loading require that the time should be scaled by a factor of SQRT (60) [5]. However, due to limitations associated with the shaker, this requirement could not be satisfied. Rather, a scale factor of 1 was used for the time scale. Comparison of the experimental and the numerical analysis of the bridge shown in later sections of this article

indicated that the results were comparable irrespective of this difference. Table 1 provides the similitude requirements for elastic vibrations along with those assumed in the current study.

A number of different sensors were employed for monitoring the response of the bridge including FBG sensors for monitoring the force in the cables. FBG sensors were also employed on the bridge deck for monitoring the flexural response of the deck (Fig. 4a). Three linear variable displacement transformers (LVDT) with a range of  $\pm 25$  mm were connected to the side surface (X–Z plane) of the mid-span, quarter span, and the mid-side-span of the



(a) Instrumentations at mid-span



(b) One fourth span

Fig. 4 Instrumentation



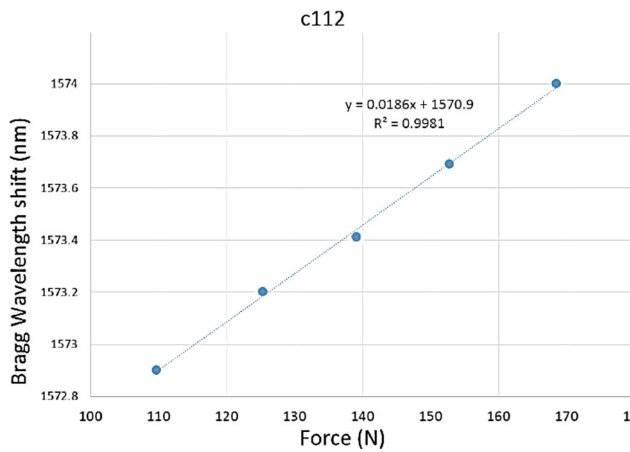


Fig. 5 FBG sensor calibration (No. c112)

bridge deck in order to measure the lateral displacements as shown in Fig. 4b. Four accelerometers were adhered to the side surfaces (XZ plane in Fig. 4a) of the deck to measure

the accelerations of the bridge as shown in Fig. 4. These measurements were employed for comparison with the computed values based on the proposed method.

The FBG sensors had a maximum strain range of approximately 6000  $\mu\epsilon$  and composed of polyimide-coated SMF-28 fibers. Figure 5 shows a typical linear calibration response of an FBG strain sensor in terms of the tension in the cables. The forces in the cables of the model bridge varied from 90 to 170 N (i.e., within the linear range of the FBGs). Figure 6 corresponds to the schematic diagram of the location of the sensors, accelerometers, shaker, and LVDTs along the span and cables of the bridge.

The seismic excitations to the bridge were applied during the experiments in the lateral direction using the seismic records of El-Centro, and Taft earthquakes. The El Centro and Taft earthquakes were selected due to immediate availability of the excitation records for the present study. The experiments also involved using white noise for exciting the bridge. The 1940 El-Centro S00E wave was

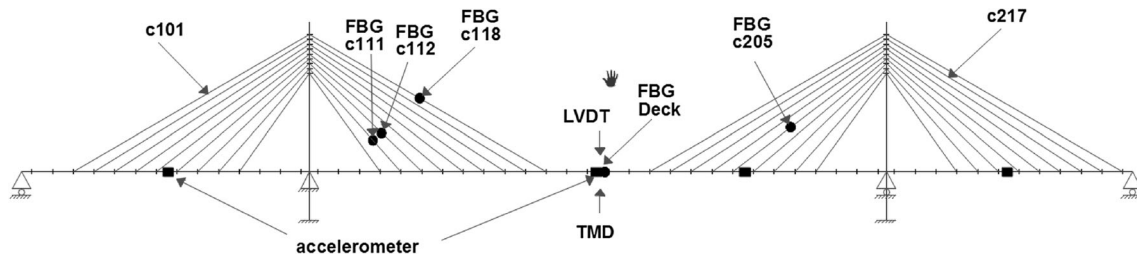
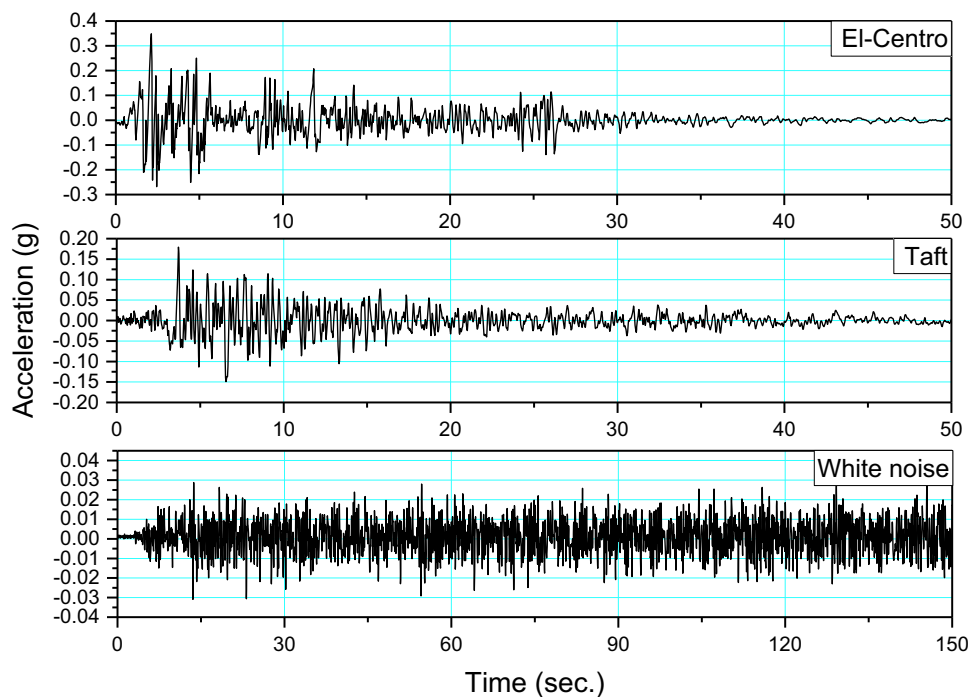
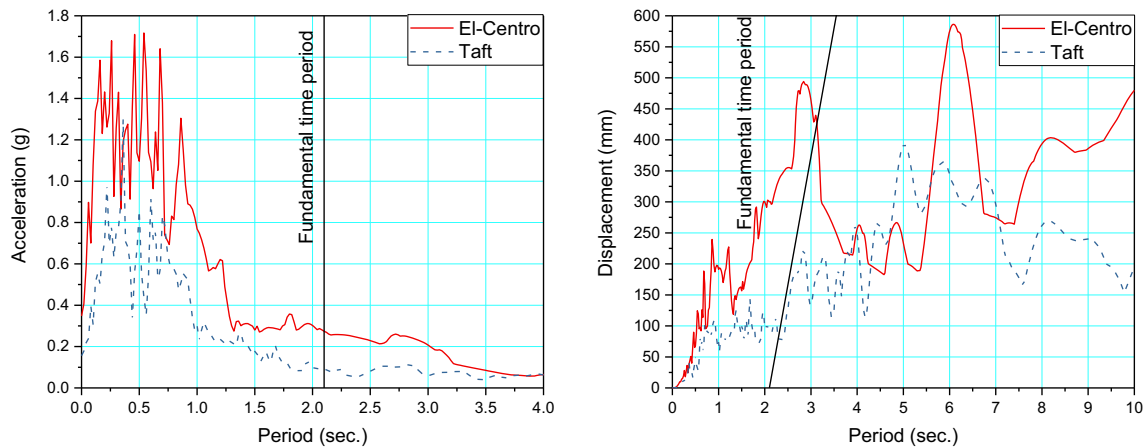


Fig. 6 Location of sensors, accelerometers, LVDTs and the shaker along the bridge span and wires

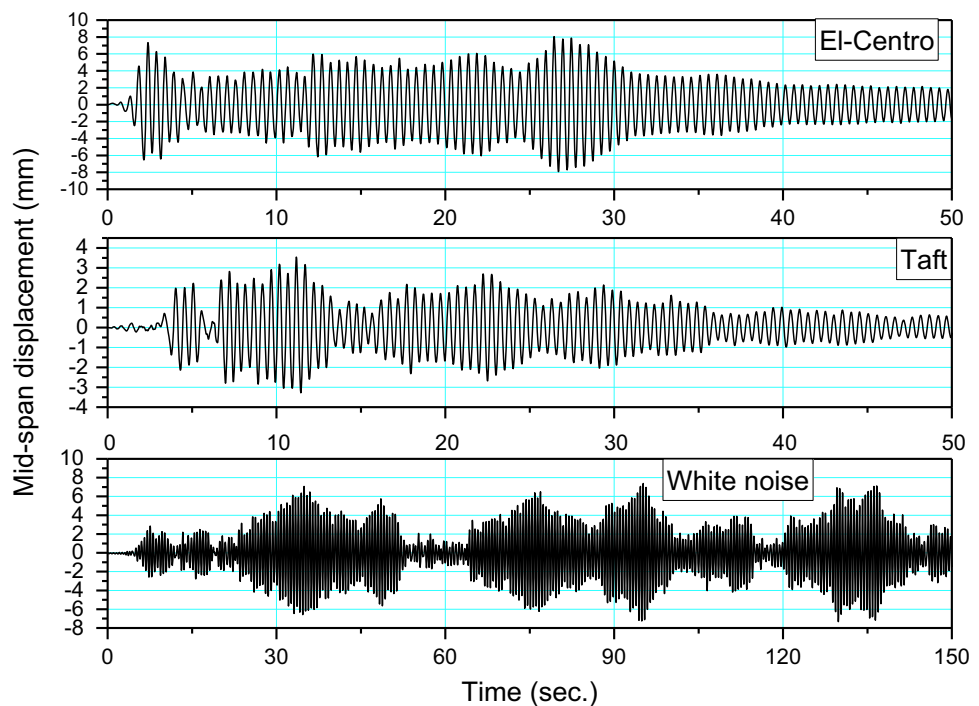
Fig. 7 Time history of El-Centro earthquake, Taft earthquake, and White noise vibration





**Fig. 8** Acceleration and displacement response spectra of El-Centro and Taft earthquakes for 0.5% damping

**Fig. 9** Mid-span displacement time history of El-Centro earthquake, Taft earthquake, and White noise vibration



recorded at the Imperial Valley in 18 May 1940, with a Peak Ground Acceleration (PGA) of 0.348 g. The 1952 Taft N21E earthquake was recorded at the Kem County in 21 July 1952. The PGA for this earthquake was of 0.156 g. The time history for both earthquakes is shown in Fig. 7. In addition to these actual earthquakes, an artificial white noise encompassing a wide range of frequencies was also used to represent a general motion for exciting all modes of vibration of the bridge (Fig. 7). The acceleration and displacement response spectra of El-Centro and Taft earthquakes are shown in Fig. 8. Moreover, Fig. 9 illustrates the lateral displacement curves obtained analytically at the mid-span during El-Centro, and Taft earthquakes, as well as those due to the white noise, respectively. These

displacement records were experimentally applied on the bridge model using the shaker shown in Fig. 10.

#### 4 Numerical analysis

A two-dimensional finite element model was constructed for the bridge. The support conditions, materials, and structural properties that were used in modeling are identical to those of the reduced-scale model described earlier in this article. Frame elements were used for modeling the pylons and the deck, and cable elements were used to model the cables. The dynamic behavior of the bridge was investigated through studying its motion and frequency



Fig. 10 Shaker connected to the bridge at mid-span

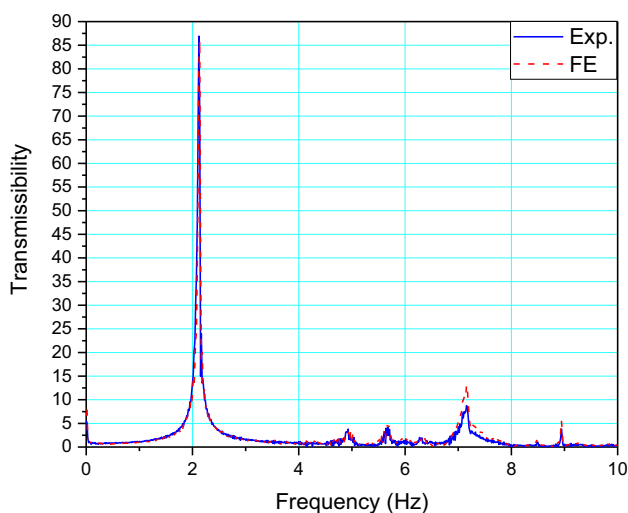


Fig. 11 FFT of acceleration at mid-span of the deck

spectra characteristics by vibration analysis. The vibration analysis was also useful in verifying the accuracy of the finite element model in comparison with the experimental results. The bridge was also excited by white noise and the modal frequencies of the bridge were obtained through Fast Fourier Transform (FFT) analysis of the acceleration at mid-span both by experimental measurements and analytical computations. Figure 11 corresponds to the comparison of the experimental and analytical frequency spectrums of the bridge. Results shown in Fig. 11 provide information about the dominant vibration frequency of the deck. The analytical and experimental results were comparable indicating the accuracy of the finite element model of the bridge.

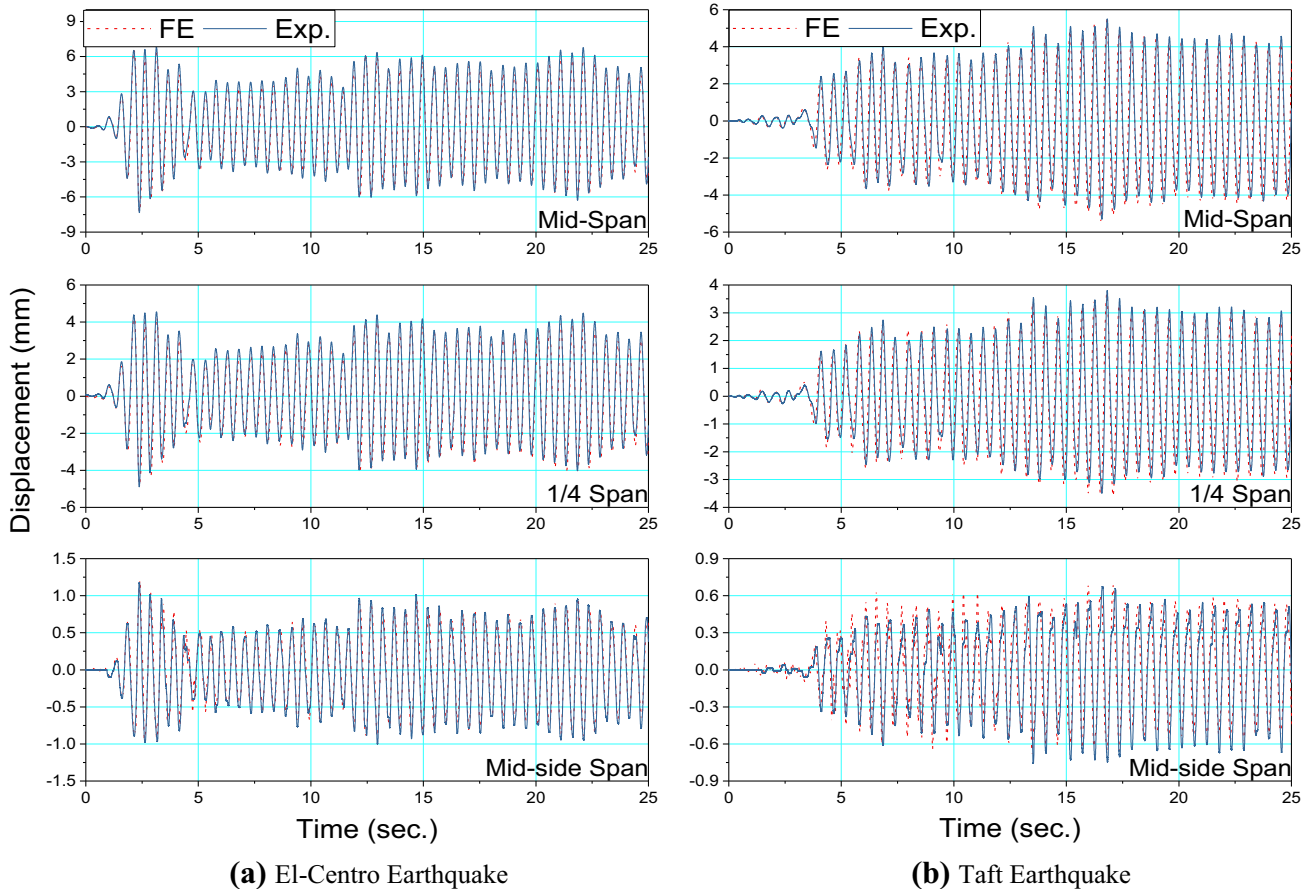
## 5 Results and discussion

Figure 12 shows comparison between experimental and analytical displacements at different locations of the bridge during El-Centro and Taft earthquakes, respectively. Results shown correspond to the comparison of the displacements during the experiments with the white noise. As shown by these results, the experimental and analytical results are comparable. Considering the fact that the analytical results mimicked the experiments very well, the finite element model was employed for the rest of the analysis of the bridge under lateral seismic excitations (Fig. 13).

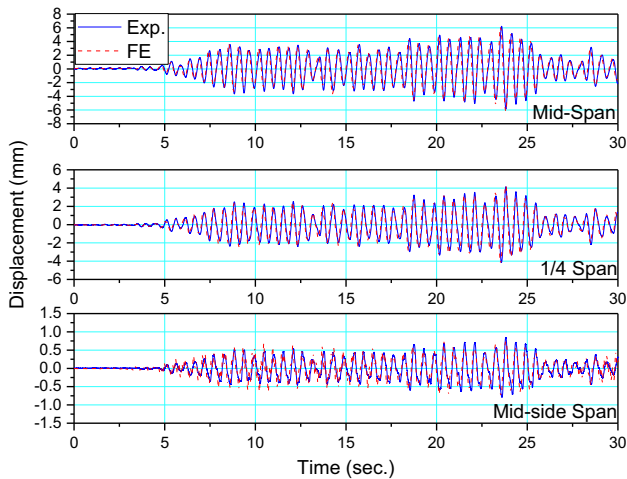
Figure 14 provides information about the first ten modes of vibration of the bridge. The fundamental mode of vibration is the oscillation of the deck in the transverse direction. Table 2 summarizes the results of the modal and cumulative modal participating mass ratios in the lateral direction for the first twenty modes of vibration. The cumulative participating mass ratio in the lateral direction is 80.24%, indicating the need to include more modes of vibration for modal analysis of the bridge. In the current study, 100 modes of vibration were taken into account in the analysis with 90.0% participation due to the above-mentioned cumulative participating mass ratio in the lateral direction.

Figure 15 pertains to some selected modes of local vibration of the cables. The longest cable vibrated in the 23rd and 24th modes taking the shape of a first mode in the in-plane and out-of-plane excitations, respectively. The same cable vibrated in an “S” shape in the 97th and 98th modes of vibration, respectively. The periods of local cable vibrations began at 0.025 s and ended at 0.0048 s. Vibration of the cables over a large spectrum are likely to encounter resonance during wind excitation with damaging effects, including fatigue at cable anchors. Figure 16 depicts the time history record of the forces in cables C111, C112, C118, and C205 obtained experimentally by the FBG sensors. The maximum, minimum, and average values for the cable forces are also shown in Fig. 16. These results indicate that the lateral earthquake excitations do not affect the cable forces in a significant manner.

Figure 17a shows the time history of the base shear at the left pylon during El-Centro and Taft earthquakes. In addition, Fig. 17b corresponds to the distribution of the envelope of the shear forces over the height of the left pylon during El-Centro and Taft earthquakes, respectively. The maximum base shear is close to 0.012 kN in the model structure, representing approximately 43.2 kN in the prototype structure. Such small value of the base shear is unlikely to result in any plastic action in the pylon of the actual bridge. Figure 17c pertains to the envelope of the



**Fig. 12** Comparison of experimental and analytical displacements at different locations of the bridge during



**Fig. 13** Comparison of experimental and analytical displacements at different locations of the bridge during White noise vibration

moments in the left pylon during El-Centro and Taft earthquakes. The maximum bending moment is 22 N-m at the base of the pylon. The corresponding value in the

prototype is 4750 kN-m. This value of moment acts on the whole section of the pylon just above the support. The computations did not include a detailed stress analysis for the pylon. However, it is expected that the large magnitude of the maximum moment at the base could lead to inelastic action at the section.

Figure 18 corresponds to the distribution of the envelope of the shear forces and bending moments in the deck for the El-Centro and Taft earthquakes. The deck strains due to the El Centro earthquake are larger than the strain response due to the Taft earthquake. This agrees with the response spectra curves of both earthquakes shown earlier in Fig. 8. It is also noticed that the maximum moments occur at the middle of the central span followed by the moments at the location of the pylons on the deck. On the other hand, the maximum shear forces acting on the deck occur in the intermediate spans at the locations of the pylons. Considering these results, it is reasonable to conclude that the most critical sections of the deck are those located at the ends of the intermediate span where a combination of both high values of moments and shears occur.



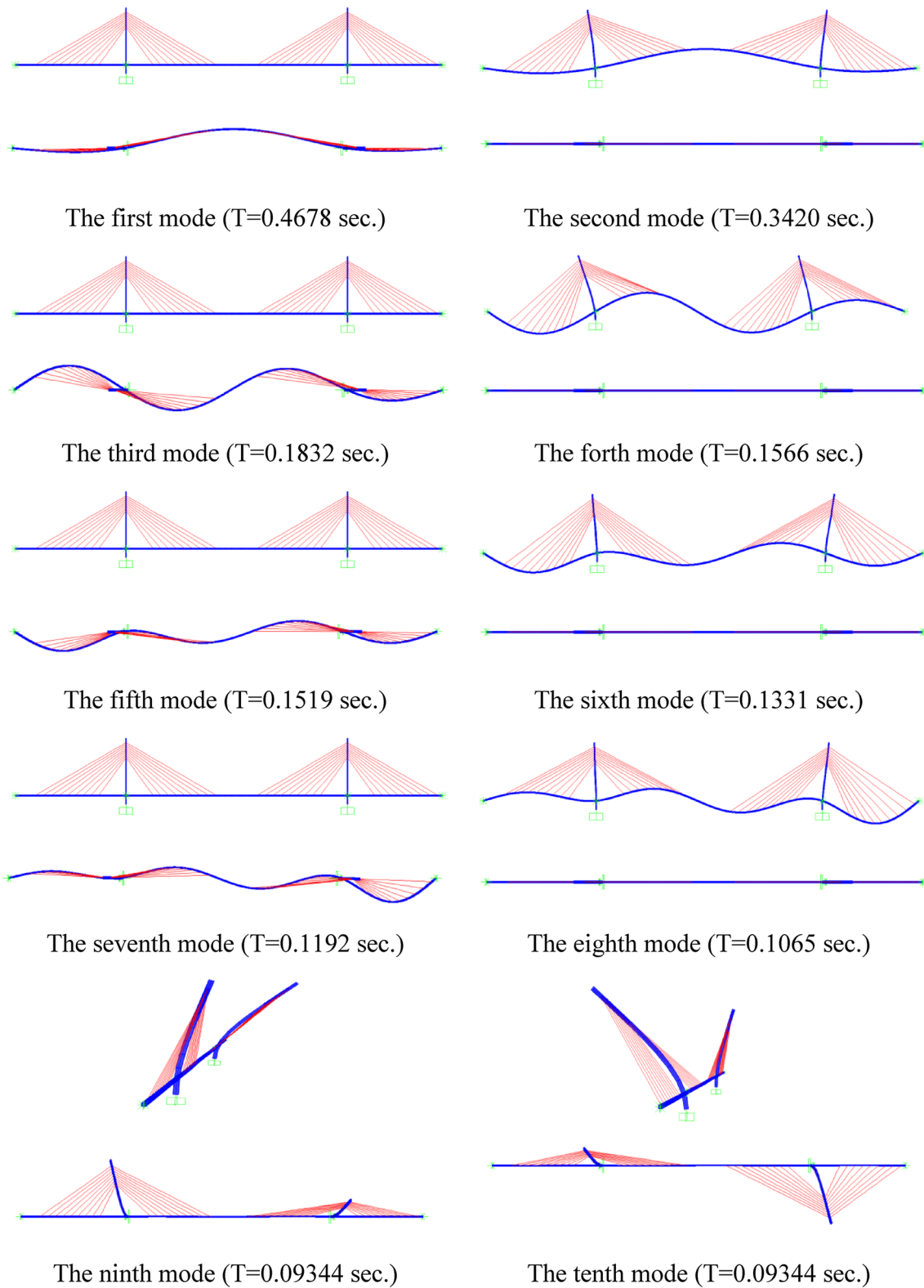


Fig. 14 Analytical mode shapes of the bridge model

**Table 2** Cumulative modal participating mass ratios in the lateral direction, 20 modes (%)

Mode no.	Period (s)	Modal participating mass ratios in the lateral direction (%)	Cumulative modal participating mass ratios in the lateral direction (%)	Nature of modes of vibration
1	0.468	28.12	28.12	Transverse bending of deck
2	0.342	0.00	28.12	Vertical bending of deck
3	0.183	5.40	33.51	Transverse bending of deck
4	0.157	0.00	33.51	Vertical bending of deck
5	0.152	19.10	52.61	Transverse bending of deck
6	0.133	0.00	52.61	Vertical bending of deck
7	0.119	8.66	61.27	Transverse bending of deck
8	0.106	0.00	61.27	Vertical bending of deck
9	0.093	5.14	66.42	Transverse bending of pylons
10	0.093	1.00	67.42	Transverse bending of pylons
11	0.081	12.49	79.90	Transverse bending of deck
12	0.075	0.00	79.90	Vertical bending of deck
13	0.061	0.00	79.90	In-plane bending of pylons
14	0.060	0.00	79.90	In-plane bending of pylons
15	0.052	0.21	80.11	Transverse bending of deck
16	0.048	0.00	80.11	Vertical bending of deck
17	0.046	0.06	80.17	Transverse bending of deck
18	0.044	0.00	80.17	Vertical bending of deck
19	0.036	0.06	80.24	Local transverse bending of the right side span
20	0.035	0.00	80.24	Local vertical bending of the right side span
.	.	.	.	.
.	.	.	.	.
100	0.0126	$4.93 \times 10^{-15}$	90.01	S-shape vibration of Cable No. c101

The value of the maximum moment at the middle of the mid-span is 130 N-m. The nominal moment capacity of this section was computed to be 3000 N-m. Therefore, the scaled model bridge behaved essentially elastic during these excitations. The corresponding value of the actual moment acting on the mid-span section is  $28 \times 10^3$  kN-m in the prototype bridge. This value is still below the elastic capacity of the deck. The maximum shear force in the deck of the model structure is 120 N. The nominal shear capacity is 60 kN, which confirms the elastic behavior. The corresponding value of shear force acting on the prototype bridge is 430 kN. Such value of shear force acting on the deck of the prototype bridge is considered insignificant.

The time history record of the mid-span strain during El-Centro and Taft excitations is shown in Fig. 19. The maximum recorded strain is  $0.7 \mu\epsilon$ , which is a small strain indicating essentially elastic behavior of the model. This is attributed to the high nominal moment capacity of this section (3000 N-m). Finally, the time history of the lateral displacement of the top of the pylon during El-Centro and Taft earthquakes was obtained and is shown in Fig. 20.

This figure also shows the envelope of the pylon displacements along the height of the pylon due to El-Centro and Taft earthquakes. The maximum displacement is 0.28 mm in the model which corresponds to about 17 mm in the prototype bridge. This is negligible because the maximum pylon displacement represents only 0.012% of the pylon height.

## 6 Conclusions

The structural response of cable-stayed bridges under the effect of lateral earthquake excitations is studied herein. The performance of the bridge was evaluated based on experimental and analytical measurements of the bridge responses. Key response parameters included forces in cables, strains and stresses in the deck, as well as moments and shear forces acting on the pylons in the transverse directions. Although, not all of the elastic model similitude requirements were exactly satisfied, the results of this study provided sufficient insight into the structural behavior of

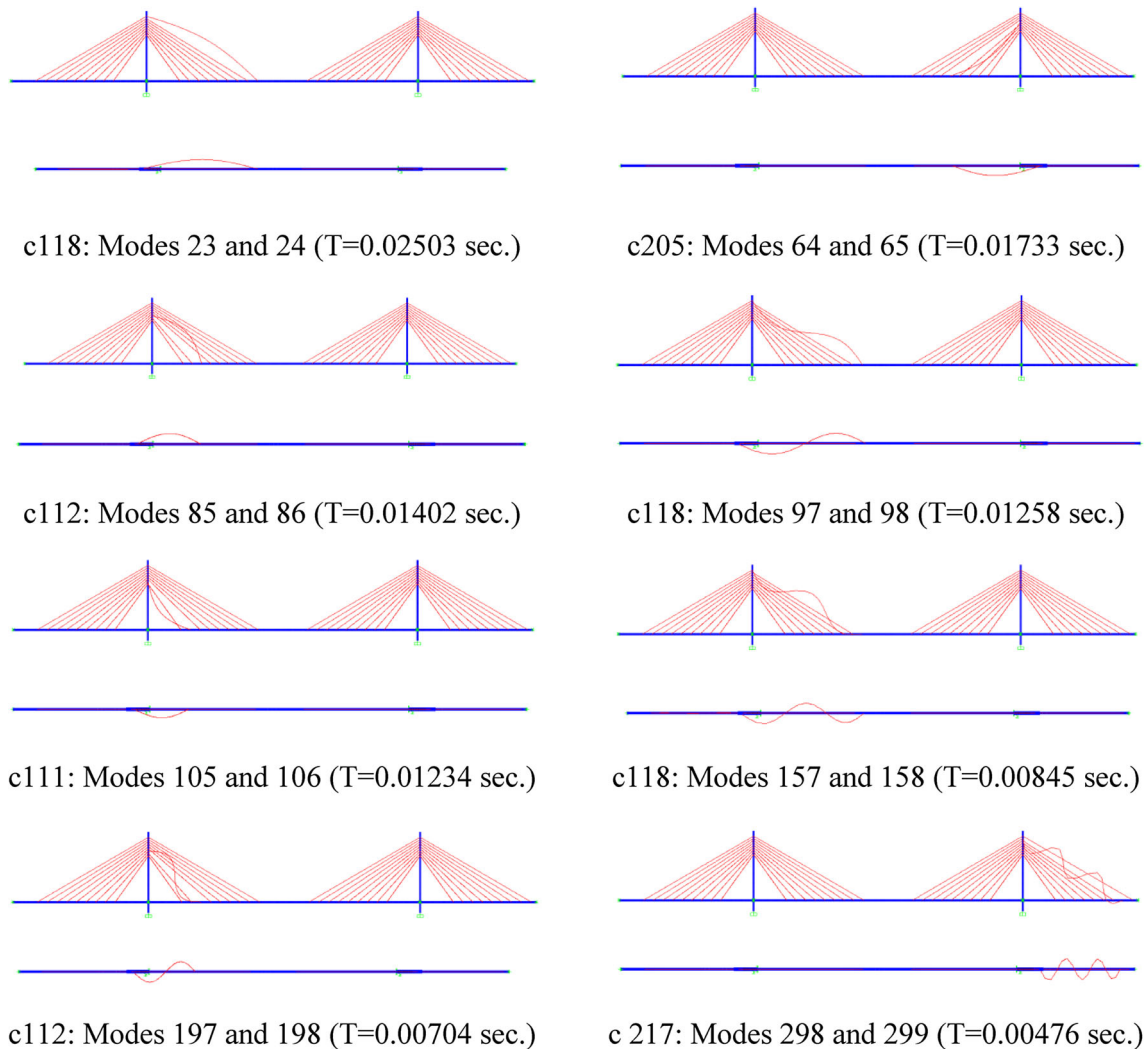


**Fig. 15** Selected analytical mode shapes of the bridge cables

the prototype bridge. For example, the difference in the time scale may induce errors in the interpretation of the results when applied to the actual bridge. The numerical–experimental approach was employed in order to evaluate the correspondence of the strains, displacements, and accelerations between the numerical model and scaled model of the bridge. The correlation between the numerical and experimental response served as means for verification of the approach adapted in the present study. Based on the results obtained in this study, the following conclusions can be drawn:

1. The experimental and analytical results were comparable. Moreover, both the experimental and analytical investigations yielded the same displacements at different locations of the bridge for the seismic excitations studied here.
2. No significant effects were observed due to the lateral earthquake excitations on the forces of the cables.
3. The periods of local cable vibrations occurred over a range between 0.025 and 0.0048 s. Vibration of the cables over a large spectrum is likely to encounter resonance during wind excitations with damaging effects, including fatigue at cable anchors.

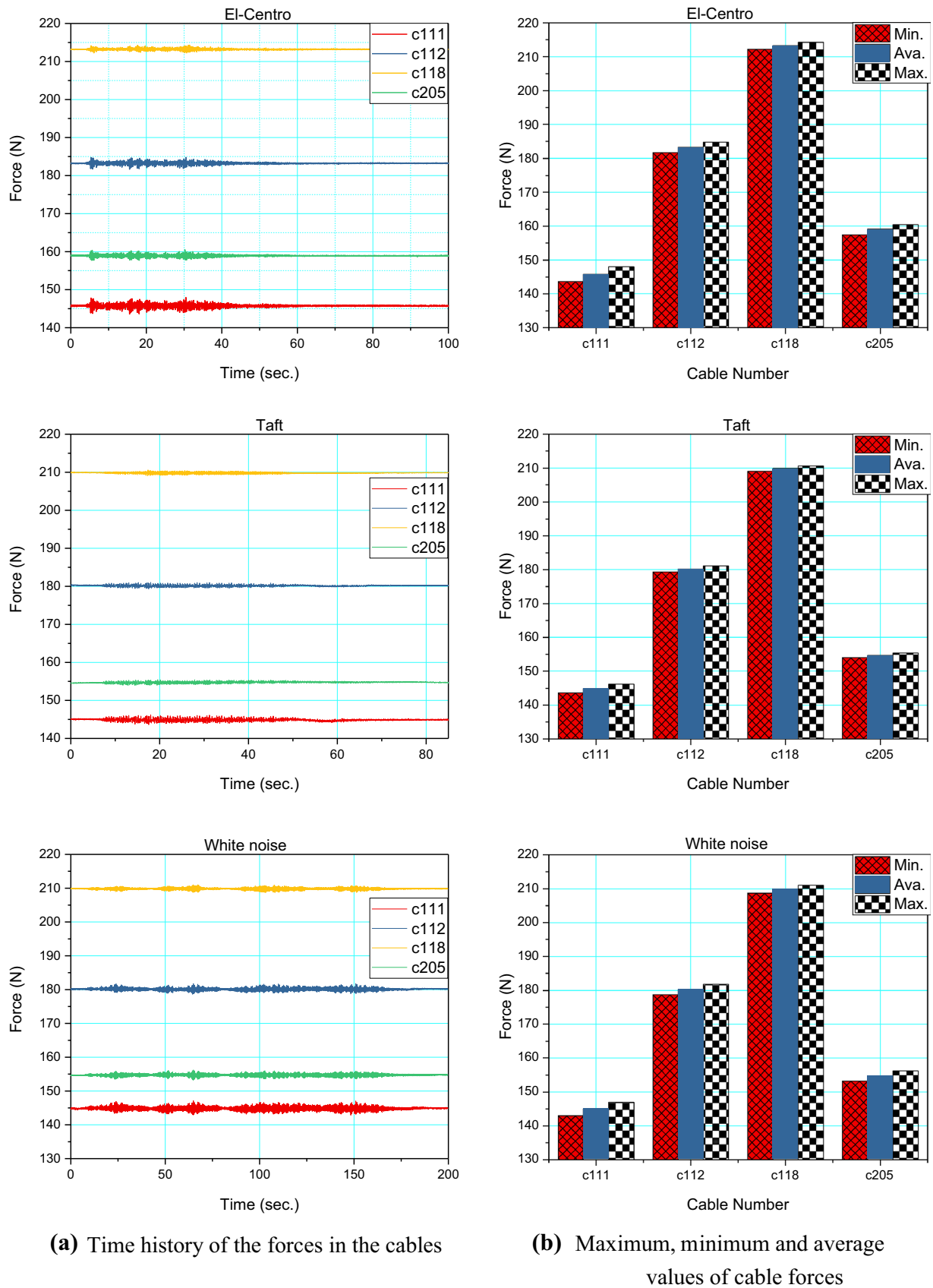
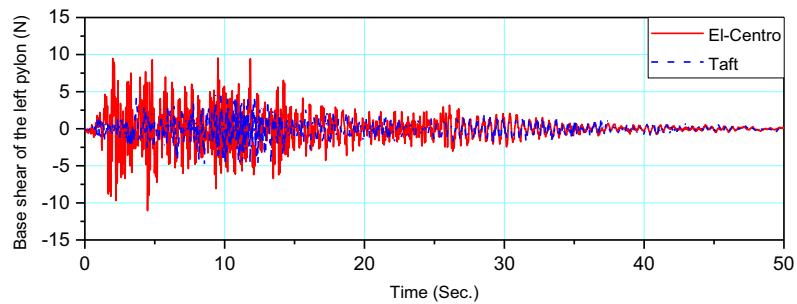


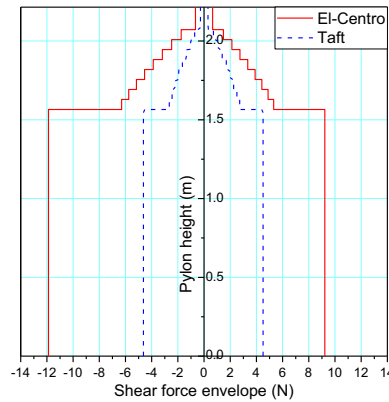
Fig. 16 Experimentally recorded forces in the cables using FBG devices



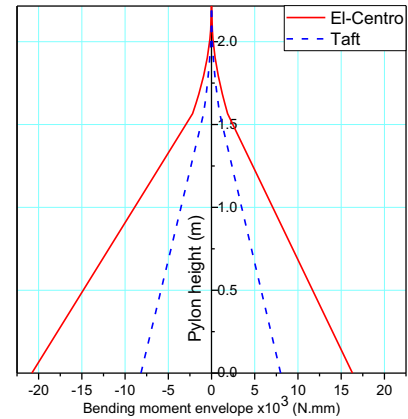
**Fig. 17** Straining actions resulting in the left pylon



**(a)** Time history of base shear at the left pylon



**(b)** Envelope of shear forces over the height of the left pylon



**(c)** Envelope of bending moments over the height of the left pylon.

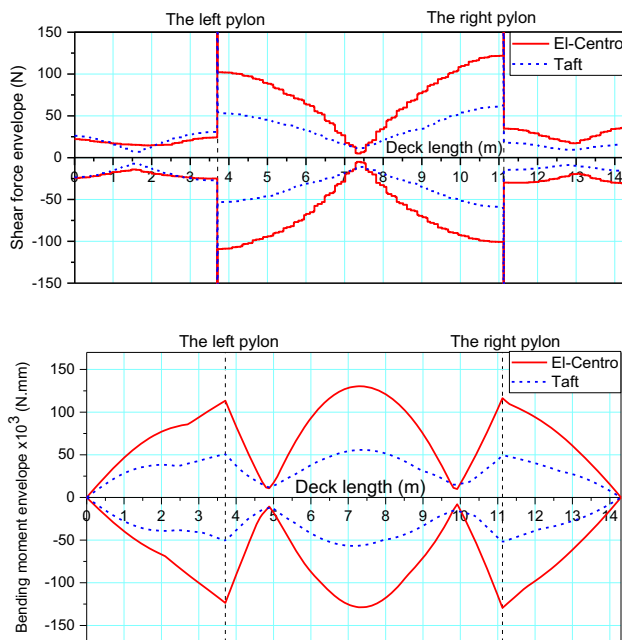
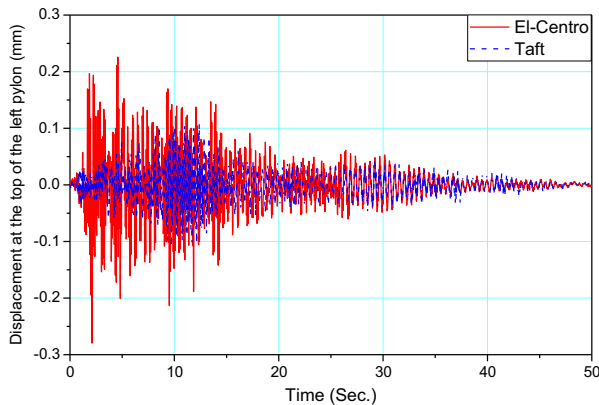
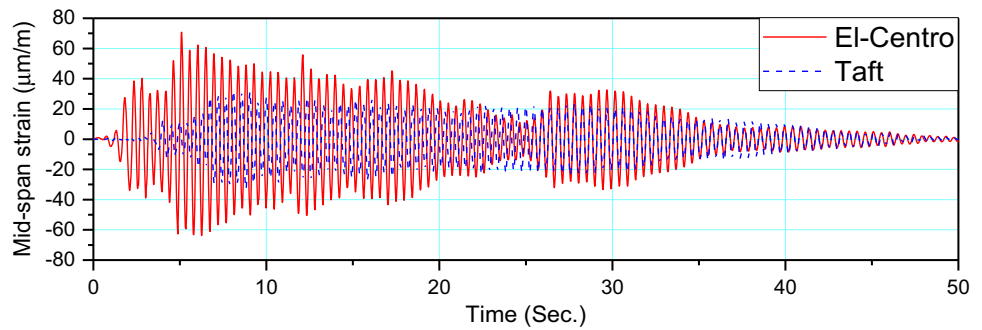


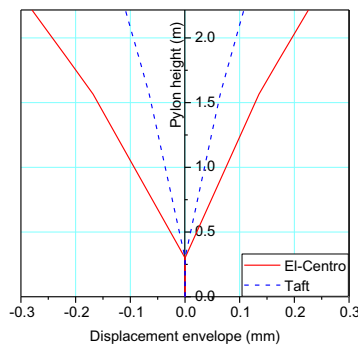
**Fig. 18** Envelope of shear forces and bending moments in the deck during El-Centro and Taft earthquakes

4. The earthquake excitations resulted in small value of equivalent base shear in the pylon of the prototype bridge which is unlikely to result in any plastic action. However, the moment acting on the base of the pylon might lead to inelastic action and should be taken into consideration during the design process.
5. The most critical sections of the deck are those located in the intermediate span at the locations of intersection with the pylon where a combination of both high values of moments and shears occur. Moreover, the high moments at the middle of the deck are associated with small values of shear forces and hence can be designed based on the value of pure moment.
6. The equivalent value of moment acting on the mid-span section of the prototype bridge is below the elastic capacity of the prototype steel deck.
7. The maximum lateral displacement of the prototype pylon is small and far less than those allowed by codes.

**Fig. 19** Time history of mid-span strain



**(a)** Time history of lateral displacement at the top of the pylon



**(b)** Envelope of pylon displacement along its height

**Fig. 20** Lateral displacement of the pylon

## References

- Caetano E, Cunha A, Taylor CA (2000) Investigation of dynamic cable-deck interaction in a physical model of a cable-stayed bridge. Part I: modal analysis. *Earthq Eng Struct Dyn* 29(4):481–498
- Camara A, Astiz MA (2012) Pushover analysis for the seismic response prediction of cable-stayed bridges under multi-directional excitation. *Eng Struct* 41:444–455
- Camara A, Efthymiou E (2016) Deck-tower interaction in the transverse seismic response of cable-stayed bridges and optimum configurations. *Eng Struct* 124:494–506
- Chang KC, Mo YL, Chen CC, Lai LC, Chou CC (2004) Lessons learned from the damaged Chi-Lu cable-stayed bridge. *J Bridge Eng* 9(4):343–352
- Harris HG, Sabnis G (1999) Structural modeling and experimental techniques. CRC Press, LLC, Boca Raton, Florida
- Hu J, Lam H-F, Yang J-H (2018) Operational modal identification and finite element model updating of a coupled building following Bayesian approach. *Struct Control Health Monit* 25(2)
- Iranmanesh A, Ansari F (2014) Energy-based damage assessment methodology for structural health monitoring of modern reinforced concrete bridge columns. *J Bridge Eng* 19(8)
- Kalooop MR, Hu JW, Sayed MA, Seong J (2016) Structural performance assessment based on statistical and wavelet analysis of acceleration measurements of a building during an earthquake. *Shock Vib*
- LeBeau KH, Wadia-Fascetti SJ (2007) Fault tree analysis of Schoharie Creek Bridge collapse. *J Perform Constr Facil* 21(4):320–326
- Li H, Ou JP (2016) The state of the art in structural health monitoring of cable-stayed bridges. *J Civ Struct Health Monit* 6(1):43–67
- Liu WQ, Xu XL, Wang RG, Wang ZJ, Wu XL (2006) Vibration reduction design of the Hangzhou Bay cable-stayed bridges. *Struct Eng Mech* 24(3):339–354
- Nazarian E, Ansari F, Azari H (2016) Recursive optimization method for monitoring of tension loss in cables of cable-stayed bridges. *J Intell Mater Syst Struct* 27(15):2091–2101
- Nazarian E, Ansari F, Zhang XT, Taylor T (2016) Detection of tension loss in cables of cable-stayed bridges by distributed monitoring of bridge deck strains. *J Struct Eng* 142(6)
- Salem HM, Helmy HM (2014) Numerical investigation of collapse of the Minnesota I-35 W bridge. *Eng Struct* 59:635–645
- Scarella A, Salamone G, Babanajad SK, De Stefano A, Ansari F (2017) Dynamic brillouin scattering-based condition assessment of cables in cable-stayed bridges. *J Bridge Eng* 22(3)
- Siringoringo DM, Fujino Y (2006) Observed dynamic performance of the Yokohama-Bay Bridge from system identification using seismic records. *Struct Control Health Monit* 13(1):226–244
- Talebinejad I, Fischer C, Ansari F (2011) Numerical evaluation of vibration-based methods for damage assessment of cable-stayed bridges. *Comput Aided Civ Infrastruct Eng* 26(3):239–251
- Tian ZY, Lou ML (2014) Traveling wave resonance and simplified analysis method for long-span symmetrical cable-stayed bridges under seismic traveling wave excitation. *Shock Vib*
- Wang FY, Xu YL, Sun B, Zhu Q (2018) Updating multiscale model of a long-span cable-stayed bridge. *J Bridge Eng* 23(3)
- Xing CX, Wang H, Li AQ, Xu Y (2014) Study on wind-induced vibration control of a long-span cable-stayed bridge using TMD-type counterweight. *J Bridge Eng* 19(1):141–148

**Publisher's Note** Springer Nature remains neutral with regard to jurisdictional claims in published maps and institutional affiliations.